MNRAS **471,** 478–490 (2017)
Advance Access publication 2017 June 26
doi:10.1093/mnras/stx1586

The MEGaN project – I. Missing formation of massive nuclear clusters and tidal disruption events by star clusters–massive black hole interactions

M. Arca-Sedda[1,2★] and R. Capuzzo-Dolcetta[1]

[1]*Department of Physics, Sapienza, University of Rome, Piazzale Aldo Moro 5, I-00185 Rome, Italy*
[2]*Zentrum für Astronomie der Universität Heidelberg, Astronomisches Rechen-Institut, Mönchhofstr. 12-14, D-69120 Heidelberg, Germany*

Accepted 2017 June 21. Received 2017 June 20; in original form 2017 March 6

ABSTRACT

We investigated the evolution of a massive galactic nucleus hosting a supermassive black hole (SMBH) with mass $M_{\rm SMBH} = 10^8\,{\rm M}_\odot$ surrounded by a population of 42 heavy star clusters (globular clusters, GCs). Using direct *N*-body modelling, we show here that the assembly of a nuclear star cluster (NSC) through GC orbital decay and merger is efficiently inhibited by the tidal forces exerted from the SMBH. The GC mass-loss induced by tidal forces causes a significant modification of their mass function, leading to a population of low-mass ($<10^4$) clusters. None the less, the GC debris accumulated around the SMBH give rise to well-defined kinematical and morphological properties, leading to the formation of a disc-like structure. Interestingly, the disc is similar to the one observed in the M31 galaxy nucleus, which has properties similar to our numerical model. The simulation produced a huge amount of data, which we used to investigate whether the GC debris deposited around the SMBH can enhance the rate of tidal disruption events (TDEs) in our galaxy inner density distribution. Our results suggest that the GC disruption leads to a TDE rate of $\sim 2 \times 10^{-4}$ yr^{-1}, about an order of magnitude larger than observed in galactic nuclei with similar density profiles and central SMBH. Our results suggest that the GC disruption shapes the SMBH neighbourhoods, leading to a TDE rate of $\sim 2 \times 10^{-4}$ yr^{-1}, a value slightly larger than what expected in previous theoretical modelling of galaxies with similar density profiles and central SMBHs. The simulation presented here is the first of its kind, representing a massive galactic nucleus and its star cluster population on scales $\sim$100 pc.

Key words: black hole physics – stars: kinematics and dynamics – galaxies: evolution – galaxies: nuclei – quasars: supermassive black holes – X-rays: bursts.

1 INTRODUCTION

In the last 20 yr, the *Hubble Space Telescope* discovered the existence of very dense and bright nuclei in the centre of many galaxies, called nuclear star clusters (NSCs) or 'resolved stellar nuclei', with masses up to $10^8\,{\rm M}_\odot$ (Böker et al. 2002; Côté et al. 2006; Graham & Spitler 2009).

NSCs are found in galaxies of all the Hubble types (Böker et al. 2004; den Brok et al. 2014; Georgiev & Böker 2014; Turner et al. 2012), and are characterized by a complex star formation history (Rossa et al. 2006; Walcher et al. 2006).

Very often, galactic nuclei contain at their centre supermassive black holes (SMBHs), with masses in the range 10^6–$10^{10}\,{\rm M}_\odot$ (Urry & Padovani 1995; Shankar, Weinberg & Miralda-Escudé 2009; Graham et al. 2011; van den Bosch et al. 2012; Emsellem 2013; Kormendy & Ho 2013; Merritt 2013).

While the nuclei of fainter galaxies, with masses below or around $10^{10}\,{\rm M}_\odot$, seem to be dominated by the presence of an NSC, heavier ones, with masses above $10^{11}\,{\rm M}_\odot$ seem to contain only SMBHs. Within these limiting values, instead, SMBHs and NSCs co-exist (Seth et al. 2008; Leigh, Böker & Knigge 2012; Scott & Graham 2013), thus suggesting that NSC-dominated and SMBH-dominated galaxies constitute a continuous sequence (Bekki & Graham 2010). Due to this, NSCs and SMBHs are often referred to as central massive objects (CMOs).

The existence of scaling relations between SMBHs, NSCs and their host galaxies can give clues about their formation history and evolution. A widely studied relation connects the host galaxy velocity dispersion (σ_g) and the CMO mass, the so-called M–σ_g relation.

Ferrarese et al. (2006) supported an SMHB M–σ_g relation characterized by a steep slope ($M \propto \sigma_g^\alpha$; $\alpha \simeq 4$) whereas for

★ E-mail: m.arcasedda@ari.uni-heidelberg.de

NSCs, it is quite shallower, with $\alpha \simeq 2$ (Erwin & Gadotti 2012; Graham 2012; Leigh et al. 2012; Georgiev et al. 2016; Melo & Capuzzo-Dolcetta 2016). This would suggest that the two classes of massive objects follow two different evolutionary pathways.

Actually, regarding NSCs, there are two main possible, and debated, formation mechanisms: (i) the '*in situ*' scenario, in which an NSC is thought to form through a series of episodic gas infalls that could drive the formation of an SMBH (Davies, Miller & Bellovary 2011), or accretes on to it (King 2003; Milosavljević 2004; King 2005; McLaughlin, King & Nayakshin 2006; Bekki 2007; Nayakshin, Wilkinson & King 2009; Hopkins & Quataert 2010b; Aharon & Perets 2015; Antonini, Barausse & Silk 2015); (ii) the 'dry-merger' scenario, in which massive globular clusters (GCs) sink towards the galactic centre due to the action of dynamical friction (df) and merge, giving rise to the formation of an NSC (Tremaine 1976; Capuzzo-Dolcetta 1993; Capuzzo-Dolcetta & Miocchi 2008; Antonini et al. 2012; Antonini 2013; Arca-Sedda & Capuzzo-Dolcetta 2014a).

Using theoretical and statistical approaches, many authors have shown that the dry-merger scenario allows us to draw quantitatively scaling relations among the NSC properties and those of their host galaxy that well fit the observational correlations (Antonini 2013; Arca-Sedda & Capuzzo-Dolcetta 2014b; Gnedin, Ostriker & Tremaine 2014).

Moreover, the inspiralling and merger of GCs in a galaxy have found a significant support by very recent finding of RR Lyrae stars in the centre of our Galaxy (Minniti et al. 2016)

Using observational data of the dwarf starburst galaxy Henize 2-10, which hosts an SMBH surrounded by 11 massive clusters (Reines & Deller 2012; Nguyen et al. 2014), Arca-Sedda et al. (2015) have shown that the formation of an NSC is regulated by the gravitational galactic field and the SMBH, and it can occur on relatively short time-scales, <1 Gyr. Since the Henize 2-10 clusters are young, with ages $\sim$5 Myr (Chandar et al. 2003), these results suggest that NSCs can form on time-scales compatible with the SMBH growth.

The dry-merger scenario seems to explain the absence of nucleated regions in dwarf spheroidal galaxies (dSph), where SMBHs are absent, and can provide clues on their DM content, as recently shown by Arca-Sedda & Capuzzo-Dolcetta (2016, 2017).

As pointed out above, NSCs seem to disappear when the host galaxy mass, M_g, exceeds $\sim 10^{11}$ M$_\odot$ (Ferrarese et al. 2006). Moreover, the transition between NSC- and SMBH-dominated galaxies occurs when their masses equal (Neumayer & Walcher 2012; Arca-Sedda & Capuzzo-Dolcetta 2014b). Therefore, it is possible to determine a mass threshold for the central SMBH above which NSCs cannot form, which is $M_{\rm SMBH} \gtrsim 10^8$ M$_\odot$ (Antonini 2013; Arca-Sedda & Capuzzo-Dolcetta 2014b).

Recently, Arca-Sedda, Capuzzo-Dolcetta & Spera (2016) have shown that the tidal torques exerted by the SMBH can quench the formation of an NSC if the time-scale over which the SMBH grows is significantly shorter than the GC (formation + df) time-scale. Let us note that multiple GC scattering over the SMBH could produce several detectable phenomena, such as the ejection of high and hyper-velocity stars (HVSs) (Capuzzo-Dolcetta & Fragione 2015; Arca-Sedda et al. 2016; Fragione, Capuzzo-Dolcetta & Kroupa 2017), or tidal disruption events (TDEs).

As opposed to NSC dry-merger scenario, some authors proposed that the absence of nucleated regions in heavy galactic nuclei is due to the *scouring* of the nucleus operated by SMBH binary systems. Indeed, during multiple galaxy mergers, the SMBHs hosted in the galactic nuclei are brought together, and their mutual interaction excavates the merger product nucleus. This causes a mass deficit in the innermost galactic region, which depends on the SMBH final mass and the number of merging experienced by the host galaxy (Merritt 2006). Moreover, stalled satellites can further enlarge the size of the galaxy core, although the origin of such satellites can be related to multiple SMBHs, debris of a minor merger event or massive star clusters (Bekki & Graham 2010; Bonfini & Graham 2016; Dosopoulou & Antonini 2017, Donnari, Arca-Sedda & Graham, in preparation).

However, it is worth noting that these two mechanisms do not necessarily act in competition, as they operate on two different time-scales. Indeed, if the post-merged galaxy contains a population of massive star clusters, after the black hole binary (BHB) merger they can undergo df and accumulate into the galactic centre, contributing to the NSC assembly as occur in lighter galaxies. On the other hand, if the final SMBH and the galaxy are sufficiently massive and dense, their tidal forces can disrupt the infalling clusters and quench the NSC formation. In this regard, E+A galaxies are particularly interesting objects. Indeed, these E/S0 galaxies are thought to underwent a starburst $\sim$1 Gyr triggered by a merger event (Dressler & Gunn 1983; Zabludoff et al. 1996; Quintero et al. 2004). Recent observations suggest that some of these galaxies host a population of young massive clusters formed during and immediately after the post-starburst phase (Yang et al. 2004). Therefore, E+A galaxies seem to be the perfect example of post-merged systems in which star clusters orbital evolution may contribute, or not, to the formation of a bright nucleus.

In this context, we present a direct *N*-body modelling of a massive galactic nucleus ($M_g = 10^{11}$ M$_\odot$) containing 42 GCs with masses in the range 3×10^5–2×10^6 M$_\odot$ and an SMBH of mass 10^8 M$_\odot$. The results of the simulations allowed us to draw the GC orbital evolution and the SMBH role at an unprecedented level of detail, thus representing reliably the interplay between the SMBH and its neighbourhood.

In particular, we focused our attention on several key aspects of galactic nucleus evolution:

(i) possible formation of a massive NSC;
(ii) production of high (hyper)-velocity stars during the GCs–SMBH gravitational collisions;
(iii) probability of having TDEs after GCs–SMBH interactions;
(iv) ejection of black hole binaries (BHBs) from the GC cores during their infall and possible decrease of their coalescence time-scale;
(v) interaction between the central SMBH and intermediate mass black holes (IMBHs) transported within the infalling GCs;
(vi) implications for extreme mass-ratio inspirals (EMRIs);

This paper is intended as the first of a series of three which would deepen the points indicated above. This Paper I aims at investigating the direct consequence of the GC orbital evolution in the combined galaxy+SMBH field to the spatial and kinematical structure of the inner galactic part. The other papers will mainly deal with, respectively, the formation of BHBs and their eventual coalescence and the possible effects of IMBHs on the SMBH dynamical evolution (Paper II) and the topics of the HVS generation (Paper III).

The paper is organized as follows: in Section 2, we introduce the galaxy model and the GC orbital and structural properties; in Section 3, we introduce the results of the numerical simulation with particular focus on the competing action of dynamical friction and tidal disruption processes; in Section 4, we discuss some implications of our results: in particular we show in Section 4.1 that the GC orbital evolution does not drive the formation of an observable NSC

when the SMBH is as massive as the one considered here while in Section 4.2, we focus the attention on the impact of GC–SMBH interaction in favouring or preventing TDEs; and finally, Section 5 is devoted to the conclusions.

2 MODEL

In this work, we simulated the evolution of 42 GCs moving in the inner region of a galaxy hosting an SMBH with mass 10^8 M$_\odot$. The simulation has been performed in the framework of the '*Modelling the Evolution of Galactic Nuclei*' (MEGaN) project.

We model the galaxy and the clusters by particles, finding a good balance between the total computational load and the reliability of the system representation.

To model the galaxy, we used a truncated Dehnen model (Dehnen 1993):

$$\rho_{\rm D}(r) = \frac{(3-\gamma)M_g}{4\pi r_g^3}\left(\frac{r}{r_g}\right)^{-\gamma}\left(1+\frac{r}{r_g}\right)^{-4+\gamma}, \quad (1)$$

with M_g the total galaxy mass, r_g its scale radius and γ tunes the steepness of the profile. We consider a galaxy with total mass $M_g = 10^{11}$ M$_\odot$. According to the M_g–$M_{\rm SMBH}$ relation provided by Scott & Graham (2013), such a value of M_g implies an SMBH mass of $\sim 10^8$ M$_\odot$. In order to generate a reliable model, we chose $r_g = 2$ kpc and $\gamma = 0.1$, which result in a galaxy effective radius $R_e = 5.3$ kpc. As shown by Merritt (2013), $\gamma = 0.5$ is the maximum value allowed to isotropic distribution functions around a massive black hole. Therefore, our choice of $\gamma = 0.1$ implies some anisotropy of the stars' distribution function within the SMBH influence radius.

On the other hand, galaxy merger and SMBH pairing and collisions can cause a significant flattening of the merger product density profile, leading to γ values smaller than 0.3 (Merritt 2006).

Sampling this galaxy model by particles would require $\sim 10^{11}$ particles, a number exceedingly large to be simulated even with the most advanced computational devices available on the market. Due to this, we restricted our galaxy model to the thinner 150 pc, adopting a modification of the density profile in equation (1)

$$\rho(r) = \frac{\rho_{\rm D}(r)}{\cosh(r/r_{\rm cut})}, \quad (2)$$

where $\cosh(r/r_{\rm cut})$ is the usual hyperbolic cosine function and $r_{\rm cut} = 150$ pc. This choice allows us to model the galaxy nucleus with a mass of 2.8×10^8 M$_\odot$.

We selected randomly the 42 GC masses in the range 0.3–2 $\times$ 10^6 M$_\odot$, obtaining a total mass 5×10^7 M$_\odot$ for our sample of GCs.

To model the whole system (galaxy+GCs), we used a total number of particles equal to 2^{20}. Moreover, we assumed for particles in the galaxy model an individual mass five times larger than for particles in the GCs. This choice allowed us to model the smallest cluster with more than 2000 particles, thus ensuring an evaporation time-scale, which is the time-scale over which two-body relaxation drives the GC disruption, $\simeq$3 Gyr, sufficiently longer than the simulated integration time. We performed several test runs by varying the ratio of galaxy to GC particle masses, finding that the choice of a ratio equal to 5 gives a very reliable simulation outcome.

The GC initial positions and velocities have been selected self-consistently, according to the background density distribution.

Once the GC positions have been assigned, it is possible to estimate their tidal radius, R_t, which defines the region within stars are bounded to the GC. A general way to estimate such length-scale is the following:

$$R_t = \left(\frac{GM}{\omega^2 + {\rm d}^2U/{\rm d}r^2}\right)^{1/3} \quad (3)$$

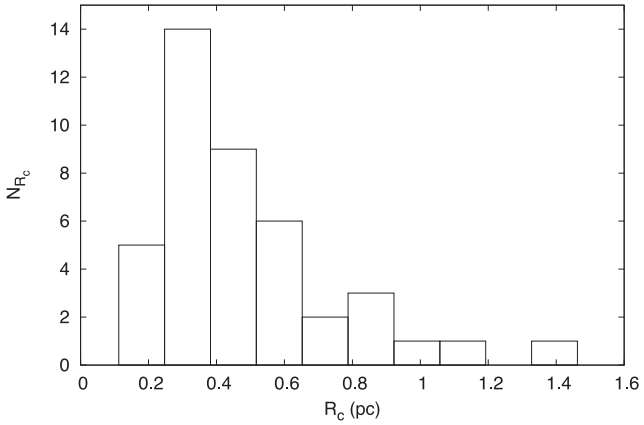

Figure 1. The GC core radius initial distribution.

Each GC has been modelled via a King density profile (King 1966), which is defined by the adimensional potential well W_0, the GC core radius R_c and its total mass M. In order to provide reliable models, we selected W_0 in the range 6–8, since only GCs with a sufficiently deep potential well can arrive near the central SMBH without being disrupted by the strong tidal forces.

The knowledge of W_0 and R_t allows us to estimate the core radius, R_c, thanks to the correlation between W_0 and the concentration parameter c, defined as $c = R_t/R_c$. Fig. 1 shows the number distribution of the core radii evaluated this way. Table 1 summarizes the main parameters of our GC models.

Our simulation has been run on two different composite platforms: (i) ASTROC9, a desktop computer hosting 2 Xeon X5650 processor and 4 RADEON HD 7990 graphic processing units (GPUs); (ii) ASTROC16a, hosting 2 Xeon E5-2623v3 and 4 NVIDIA Titan X GPUs. We used the direct N-body code `HiGPUs` (Capuzzo-Dolcetta, Spera & Punzo 2013), a highly parallel, direct summation, sixth order, Hermite integrator that implements block-time steps.

3 RESULTS

In order to follow the GC evolution, it is important to determine three important quantities: the GC centre of mass (COM), its tidal radius and its bounded mass. While this is simple for any spherically symmetric system, where the COM coincides with the centre of density (COD), for systems suffering intense tidal force, this evaluation becomes much more complicated. In our case, we developed an algorithm that uses the COM as the starting point, evaluates in a recursive way the centre of density. As shown in Arca-Sedda et al. (2016) (see their fig. 1), our approach works very well even in the case of a severely warped GC. Once the infalling GC COD is evaluated correctly, another important quantity is its tidal radius R_t. According to equation (3), its evaluation depends on the GC bounded mass, M, that in turn depends on R_t.

Therefore, to give a proper estimate of the tidal radius, we first use the total GC mass in equation (3), then we evaluate the GC mass enclosed within R_t and use it to re-estimate M. After naming M_0 the

Table 1. Properties of the GC sample.

GC name	W_0	R_t (pc)	R_c (pc)	M_{GC} 10^6 M$_\odot$	r_{GC} (pc)	v_{GC} km s^{-1}	e	t_{df} (Gyr)	$M_{GC,f}/M_{GC}$ (per cent)	N_{GC}
GC1	7.54	10.9	0.207	1.05	71.4	121	0	0.295	4.94	10 445
GC2	7.13	17	0.443	0.906	117	89.4	0.527	0.509	30.8	8995
GC3	7.66	23.8	0.424	1.68	134	87.7	0.483	0.446	46.8	16 671
GC4	7.08	13.7	0.378	1.89	74.3	115	0.974	0.0755	2.61	18 754
GC5	7.89	16.5	0.257	1.1	107	91.6	0.553	0.368	60.5	10 966
GC6	7.28	15.1	0.35	0.452	132	24.5	0.884	0.633	1.03	4492
GC7	7.71	23.2	0.397	1.69	130	93.5	0.687	0.336	6.18	16 792
GC8	7.78	20.8	0.345	1.07	136	78.2	0.177	0.804	3.95	10 634
GC9	6.88	15.2	0.477	1.87	82.6	91.3	0.32	0.204	2.67	18 554
GC10	6.58	22	0.812	1.16	140	33.6	0.785	0.432	2.35	11 560
GC11	7.33	22.6	0.502	1.25	140	86.2	0.411	0.629	3.41	12 412
GC12	7.49	16.2	0.32	1.62	92.6	93	0.478	0.239	22.6	16 054
GC13	7.27	14.9	0.347	0.85	105	78	0.129	0.618	41	8446
GC14	6.54	15.4	0.58	0.719	115	76.9	0.125	0.806	40.1	7137
GC15	6.76	25.1	0.839	1.66	142	61.4	0.29	0.586	3.2	16 530
GC16	7.74	12.7	0.214	1.28	78.4	121	0	0.305	3.84	12 716
GC17	7.01	8.78	0.257	1.86	47.7	127	0.729	0.051	22.9	18 517
GC18	6.5	5.01	0.194	0.583	40.1	131	0.561	0.0997	6.73	5791
GC19	6.45	16.6	0.665	0.834	118	69.8	0.0695	0.801	22.8	8284
GC20	6.11	14.4	0.727	0.33	139	85	0.38	1.56	48.9	3273
GC21	7.45	13.9	0.283	1.49	81.5	90.9	0.31	0.234	15.9	14 840
GC22	7.1	19.7	0.53	1.38	119	72.6	0.00601	0.599	8.1	13 721
GC23	7.14	19.1	0.497	1.7	107	93.5	0.616	0.26	0.626	16 836
GC24	6.96	11.6	0.352	1.3	71.5	122	0	0.257	12.9	12 871
GC25	6.63	16	0.574	0.613	126	83.1	0.32	0.903	15.7	6090
GC26	6.66	26.2	0.921	1.97	140	55.8	0.407	0.462	28.4	19 521
GC27	7.78	19.6	0.324	1.24	122	36.7	0.743	0.343	3.92	12 353
GC28	7.88	8.85	0.138	1.27	54.7	136	0	0.163	18	12 598
GC29	6.02	26.8	1.46	1.79	148	93.3	0.641	0.426	31.2	17 756
GC30	7.2	18.5	0.456	1.03	122	93.9	0.686	0.421	1.03	10 226
GC31	6.43	14.4	0.583	0.612	114	56.6	0.392	0.711	4.6	6073
GC32	7.57	15.1	0.284	0.845	107	77.5	0.111	0.647	14.8	8397
GC33	6.71	9.43	0.323	1.03	62.5	135	0	0.236	1.52	10 258
GC34	7.17	19.1	0.484	1.08	124	100	0.92	0.298	5.14	10 776
GC35	7.25	11.5	0.272	0.486	98	62.1	0.316	0.683	8.28	4825
GC36	7.09	19.7	0.536	1.25	122	34	0.778	0.328	8.1	12 369
GC37	6.47	24.3	0.957	1.69	137	79.6	0.217	0.576	4.11	16 787
GC38	7.6	14.5	0.268	0.334	140	85.2	0.379	1.56	8.97	3318
GC39	6.16	23.9	1.17	1.41	143	84.3	0.336	0.636	2.45	13 990
GC40	7.18	23	0.575	1.56	133	87.6	0.485	0.458	13.2	15 468
GC41	7.74	23.7	0.401	1.39	142	71.1	0.0492	0.8	31.7	13 768
GC42	7.2	4.55	0.112	0.478	38.9	141	0.781	0.0828	8.1	4747

Column 1: GCs name. Column 2: value of the adimensional potential well. Column 3: GC tidal radius. Column 4: GC core radius. Columns 5–7: GC mass, initial position and velocity. Column 8: GC orbital eccentricity. Column 9: dynamical friction time-scale according to equation (5). Column 10: GC mass percentage by the end of the simulation. Column 11: number of particles used to model the GCs.

first guess for the total mass of the GC, we followed the scheme

$$M_0 \rightarrow R_{\rm tid,0}(M_0) \rightarrow M_1(R_{\rm tid,0}) \rightarrow R_{\rm tid,1} \rightarrow ... \\ \rightarrow M_{i-1}(R_{\rm tid,i-2}) \rightarrow R_{\rm tid,i-1}(M_{i-1}) \rightarrow M_i(R_{i-1}); \quad (4)$$

which we stop when the relative variation of the GC mass falls below 0.001.

3.1 Dynamical friction and tidal disruption

During their motion, GCs undergo df, which causes their orbital decay towards the centre of the galaxy (Chandrasekhar 1943; Tremaine 1976; Capuzzo-Dolcetta 1993).

The failure of the classical treatment developed by Chandrasekhar (1943) in describing the df in a dense galactic nucleus moved several authors to develop semi-analytical treatments that have been robustly tested against numerical experiments and reproduce satisfactorily the evolution of massive satellites spiralling around dense galactic nuclei and SMBHs (Antonini & Merritt 2012; Arca-Sedda & Capuzzo-Dolcetta 2014a; Dosopoulou & Antonini 2017; Petts, Read & Gualandris 2016). The time-scale over which this process occur is well described by the following formula, deeply discussed in Arca-Sedda & Capuzzo-Dolcetta (2014a) and Arca-Sedda et al. (2015)

$$t_{\rm df}({\rm Myr}) = t_0 g(e,\gamma) \left(\frac{M_{\rm GC}}{M_g}\right)^{-0.67} \left(\frac{r_{\rm GC}}{r_g}\right)^{1.76}, \quad (5)$$

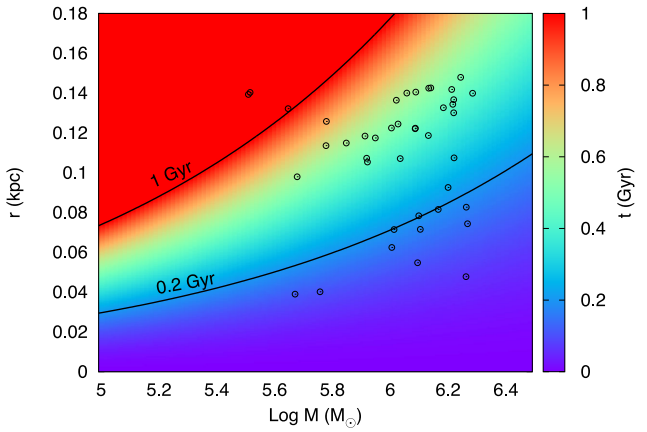

Figure 2. Colour map of the $t_{\rm df}$ at varying $M_{\rm GC}$ and $r_{\rm GC}$. Open black circles represent our modelled GCs. The map is obtained assuming an initial eccentricity $e = 0.5$. An estimate of the GC $t_{\rm df}$ is also listed in Table 1.

where $M_{\rm GC}$ is the cluster mass, $r_{\rm GC}$ its radial position within the host (spherical) galaxy and t_0 is given by

$$t_0({\rm Myr}) = 0.3 \left(\frac{r_g}{1{\rm kpc}}\right)^{3/2} \left(\frac{10^{11}{\rm M}_\odot}{M_g}\right)^{1/2}. \quad (6)$$

The function $g(e, \gamma)$ is given by

$$g(e,\gamma) = (2-\gamma)\left[a_1\left(\frac{1}{(2-\gamma)^{a_2}} + a_3\right)(1-e) + e\right], \quad (7)$$

with $a_1 = 2.63 \pm 0.17$, $a_2 = 2.26 \pm 0.08$ and $a_3 = 0.9 \pm 0.1$.

Fig. 2 shows a surface map that describes how the df time-scale varies on varying the GC mass and the initial position, according to equation (5). Our GC sample is also represented.

It is worth noting that more than 25 per cent of all the GCs have dynamical friction time-scales smaller than 200 Myr.

On the other hand, as the clusters travel within the host galaxy, the tidal torques induced by the SMBH and the galactic background induce a shattering of the incoming GCs and, in some cases, disrupt them before they approach the SMBH. We found that 57 per cent of the GCs lost more than 90 per cent of their initial mass after 223 Myr, making clear the role played by tidal heating in determining the mass deposited around the SMBH. We stopped our simulation after $\simeq$290 Myr, when the intense action of tidal forces have almost completely destroyed the GCs in our sample.

The mass-loss caused by tidal torques can be monitored assuming that the GC is at any time described by a King density profile.

Assuming a King profile, the GC mass satisfies the relation (King 1962)

$$M = \frac{R_t \sigma^2}{2G}, \quad (8)$$

where σ is the GC 1D velocity dispersion and R_t its tidal radius. Coupling equations (3) and (8) we get

$$M = \frac{\sigma^3}{2\sqrt{2}G}\left(\omega^2 + \frac{{\rm d}^2U}{{\rm d}r^2}\right)^{-1/2}, \quad (9)$$

According to our galaxy model, the gravitational potential generated by the background galaxy and the SMBH is given by

$$U = \frac{GM_{\rm SMBH}}{r} + \frac{GM_g}{(2-\gamma)r_g}\left[1 - \left(\frac{r}{r+r_g}\right)^{2-\gamma}\right]. \quad (10)$$

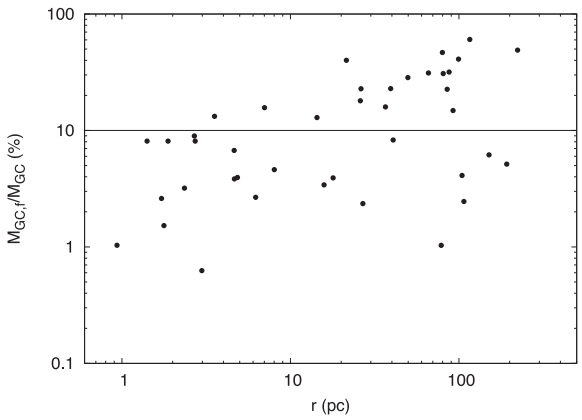

Figure 3. Percentage of the GC masses as a function of their radial distance to the central SMBH at $T = 224$ Myr.

Therefore, for a Dehnen model, we have

$$\omega^2 = \frac{GM_{\rm SMBH}}{r^3} + \frac{GM_g}{r^3}\left(\frac{r}{r+r_g}\right)^{3-\gamma}, \quad (11)$$

and

$$\frac{{\rm d}^2U}{{\rm d}r^2} = \frac{2GM_{\rm SMBH}}{r^3} - \frac{GM_g}{r^\gamma\left(r+r_g\right)^{4-\gamma}}[(1-\gamma)r_g - 2r]. \quad (12)$$

Equation (5) can be used to describe how the GC radial position r evolves as a function of the time. In particular, a GC that moves from an initial radial position r_0 to r after a time t is given by the solution of the following equation

$$t_{\rm df}(r_0) - t_{\rm df}(r) = t, \quad (13)$$

which is

$$r = r_0\left(1 - \frac{t}{t_{\rm df}(r_0)}\right)^{0.57}. \quad (14)$$

Combining equations (9)–(14) allows to obtain the time evolution of the GC mass, M. It is easily seen that

$$M = \frac{\sigma^3}{2\sqrt{2}G}\left[\frac{GM_{\rm SMBH}}{r^3}\left(1 + \frac{M_g}{M_{\rm SMBH}}\left(\frac{r}{r_g}\right)^{3-\gamma}\right)\right]^{-1/2}, \quad (15)$$

which implies

$$M \propto \left(1 - \frac{t}{t_{\rm df}(r_0)}\right)^{0.9}. \quad (16)$$

When the galaxy does not contain a central SMBH, instead, the latter equation reduces to

$$M \propto \left(1 - \frac{t}{t_{\rm df}(r_0)}\right)^{0.3\gamma}. \quad (17)$$

It should be noted that equation (9) holds only for nearly circular orbits, and under the additional assumption that the value of σ remains nearly constant along the trajectory. So, the above relations represent just a rough estimate of how much mass should be dispersed along the GC trajectory, and only detailed numerical modelling allows a detailed description of the effects of tidal forces.

Due to this, we show in Fig. 3 the percentage of the GCs bounded mass at the end of simulation. We found that more than 50 per cent of the clusters have masses smaller than 1/10th of their initial mass, thus highlighting how much tidal forces affect the growth of the galactic nucleus in this case.

It is worth noting that mass-loss significantly shapes the mass distribution of the GCs. Fig. 3 shows the GC distances to the SMBH as a function of their masses after 220 Myr. Although the correlation is very weak, it seems that the lighter the cluster, the smaller the distance to the SMBH. This behaviour seems to be at odds with the normal expectations of mass segregation, by which the most massive bodies tend to concentrate into the galactic nucleus. Actually, this plot highlights the competitive action of df and tidal heating. Indeed, df drags the most massive clusters towards the SMBH, enhancing, in turn, the tidal torque as the distance decreases. The net result is that we find the lightest clusters nearer to the SMBH while the heavier remain in an outer shell, driving the GCs in an '*anti-mass segregation*' state.

The two dominant sources of tidal forces are the central SMBH and the background galaxy. The natural length-scale over which the SMBH force dominates over the galactic background is the influence radius, given by

$$r_{\rm inf} = \frac{GM_{\rm SMBH}}{\sigma_g^2}, \tag{18}$$

with σ_g the galaxy central 3D velocity dispersion. In our model $r_{\rm inf} \simeq 13 \pm 5$ pc, therefore we expect that GCs suffer tidal forces from the SMBH only when they approach at a distance comparable to $r_{\rm inf}$. Looking at Fig. 3, it is evident that 16 out of the 42 clusters move within 10 pc, and are likely warped mostly by the SMBH. On the other hand, 9 of the remaining clusters have masses about 10 per cent of their initial values, thus pointing out the importance of the background galaxy in shaping the structural evolution of the clusters.

The combined tidal action of the SMBH and the galactic background significantly changes the GC mass distribution. Indeed, by the end of the simulation all the GCs have masses smaller than $6 \times 10^5\,{\rm M}_\odot$ the low-mass cut-off of the distribution shifts to $10^4\,{\rm M}_\odot$. Moreover, the distribution of masses above $3 \times 10^4\,{\rm M}_\odot$ is well fitted by either an exponential mass function

$$f(M) = A\exp(-M/B), \tag{19}$$

with $A = (16 \pm 2)\,{\rm M}_\odot^{-1}$ and $B = (8.2 \pm 1.2) \times 10^4\,{\rm M}_\odot$, or by a power law

$$f(M) = a\left(\frac{M}{10^5\,{\rm M}_\odot}\right)^b, \tag{20}$$

with $a = 4.2 \pm 2.0\,{\rm M}_\odot^{-1}$ and $b = -0.78 \pm 0.14$. It is worth noting that after ∼220 Myr only 17 GCs have masses above $10^5\,{\rm M}_\odot$.

This suggests that a massive galaxy likely hosts, in its nucleus, a population of relatively small GCs, characterized by the mass function shown in Fig. 4.

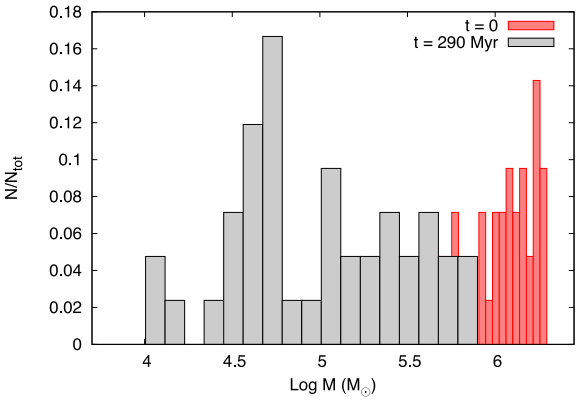

Figure 4. Distribution of masses of GCs at the beginning and the end of our simulation.

4 DISCUSSION

As we showed in the last section, the GC orbital evolution is notably shaped by the presence of the central SMBH, which has a shattering effect on them.

Several astrophysical processes can be driven by a strong SMBH–GC gravitational collision, such for instance the ejection of high-velocity stars, enhancement of stellar disruption by the SMBH. In this paper, using the data provided by our simulation, we try to determine some information about these phenomena and their consequences.

4.1 Is an NSC forming around such a massive BH?

The formation of NSCs by decay and merging of globular clusters has been tested in dwarf (Arca-Sedda & Capuzzo-Dolcetta 2016, 2017) and mid-weight galaxies (Antonini et al. 2012; Arca-Sedda & Capuzzo-Dolcetta 2014b; Mastrobuono-Battisti, Perets & Loeb 2014; Perets & Mastrobuono-Battisti 2014; Arca-Sedda et al. 2015), whereas a number of recent works have argued that this process works inefficiently in high-mass galaxies (Antonini 2013; Arca-Sedda & Capuzzo-Dolcetta 2014b; Arca-Sedda et al. 2016).

However, most of the previous works limited their models to about 10 GCs moving around an SMBH, due to the computational load required to simulate a massive galactic nucleus. In this paper, we model the entire galactic nucleus, showing that tidal forces in galaxies hosting an SMBH with mass above $10^8\,{\rm M}_\odot$ are sufficiently high to inhibit the formation of a detectable NSC.

As shown in Fig. 3, a number of GC remnants penetrate the inner region of the galaxy, reaching distances smaller than 10 pc from the SMBH. Therefore, GC debris may, in principle, leave a fingerprint in the SMBH surroundings.

Indeed, the GC evolution causes a significant flattening of the global three-dimensional velocity dispersion profile, which passes from a value, averaged over the inner 20 pc, of $\sim$500 km s^{-1} to $\sim$100 km s^{-1} by the end of the simulation. Moreover, GC orbital infall and disruption lead to an evident central increase in the spatial density profile, as shown in Fig. 5.

A relevant parameter that can be used to determine whether the GCs orbital evolution can give rise to an NSC is the amount of mass deposited around the SMBH. Fig. 6 shows the mass initially bound to the GCs, accumulated at 4, 10 and 20 pc from the SMBH as a function of the time. It is worth noting that the galaxy mass enclosed within 4 pc according to our galaxy model is $\sim 1500{\rm M}_\odot$, a value compatible with the GCS deposited mass. This would represent a first hint on the weak detectability of a possible NSC.

Observationally, an NSC in a galactic nucleus is identified as an evident edge in the host galaxy surface brightness profile (Côté et al. 2006; Turner et al. 2012; Georgiev & Böker 2014; Arca-Sedda et al. 2015). However, we did not find any evident edge neither in our model surface density profile, nor in the projected radial velocity profile, which is shown in Fig. 7. Therefore, our results suggest that the central SMBH and its surroundings act as a barrier, preventing the NSC formation and leading to an insufficient amount of GC debris around the SMBH. None the less, the interactions between

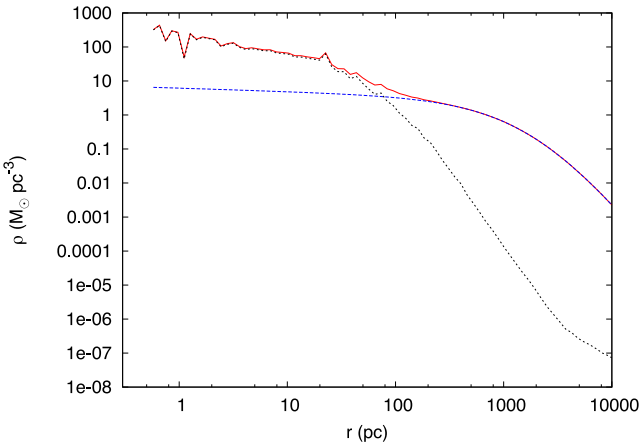

Figure 5. The blue curve is the initial galaxy density profile. The dotted curve is the GC density profile at 220 Myr, and the red curve is the global (galaxy + GC) density profile at 220 Myr.

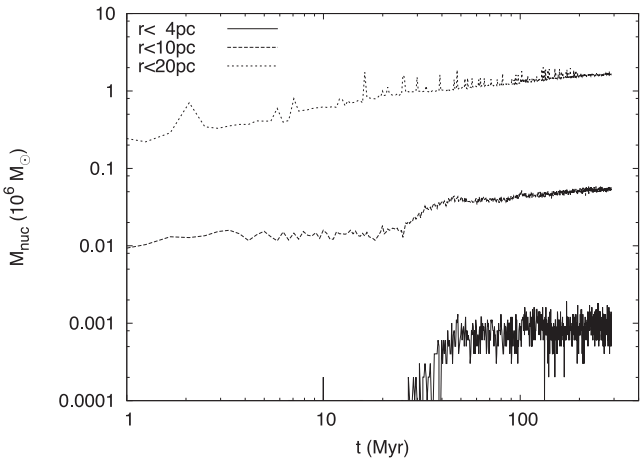

Figure 6. Time evolution of the mass deposited around the SMBH at different radii.

the SMBH and the GCs are strong enough to suggest that a number of interesting phenomena can occur, such as BHB coalescence, TDEs and GW emissions by EMRIs.

4.1.1 Central structure morphology and kinematics

In this section, we investigate the kinematical and morphological properties of the very inner region of the galaxy studied, at distances below 5 pc from the central SMBH.

In central panel of Fig. 7, we show the time evolution of the β anisotropy parameter. This parameter is defined as $\beta = 1 - (\sigma_t/2\sigma_r)^2$, where σ_t and σ_r represent the tangential and radial velocity dispersions, respectively. After ∼300 Myr, our galaxy+GCs model is characterized by $\beta \simeq 0$ within 5 pc from the SMBH, which implies an almost isotropic configuration, while it declines towards negative values outward, showing a predominance of tangential motion at the edge of the galactic nucleus.

Another important set of parameters that can be used to constrain the galaxy morphology is that of the three principal moments of inertia, $I_1 > I_2 > I_3$, which allow us to discriminate between spherical, oblate or prolate systems.

In our simulations, we found that these parameters do not vary significantly during the time evolution. In particular, the ratios I_2/I_1 and I_3/I_1 oscillate around the mean values 0.92 and 0.83, respectively.

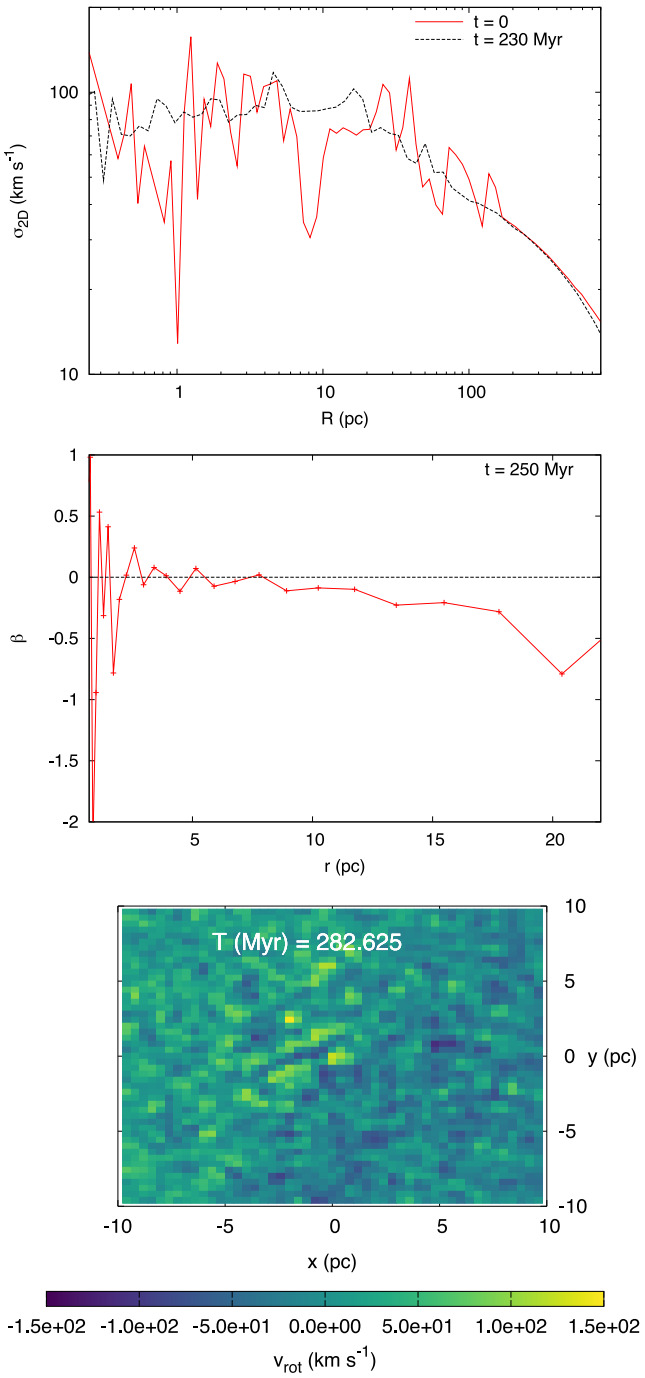

Figure 7. Top panel: surface velocity dispersion of the whole system at $T = 0$ (red straight line) and at $T = 224$ Myr (black dotted line). Central panel: the value of the anisotropy parameter β as a function of galactocentric distance at the time labelled. The dotted black line represents a zero offset. Bottom panel: mean velocity, oriented along the z-direction, within the inner 10 pc around the SMBH. A mild rotation with amplitude ∼100 km s^{-1} is evident.

A better indication on the triaxiality of a system is given by the *triaxiality parameter*, $T_{\rm tr}$, which is defined as $T_{\rm tr} = (1 - (I_2/I_1)^2)/(1 - (I_3/I_1)^2)$. According to Franx, Illingworth & Heckman (1989), $T_{\rm tr} = 0$ corresponds to an oblate configuration, whereas $T_{\rm tr} = 1$ is related to a prolate distribution. Values

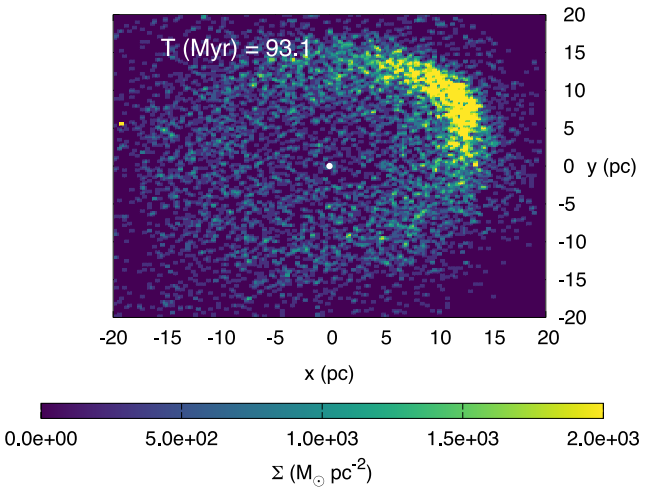

Figure 8. Surface density map in the case of a single GC moving around the SMBH with initial distance $r_0 = 50$ pc and eccentricity $e \simeq 0.7$.

in the range $0 < T_{\rm tr} < 1$ characterize triaxial-shaped systems. In our numerical modelling, we found that the region within the inner 5 pc around the SMBH is clearly triaxial configuration, reaching the value $T_{\rm tr} \simeq 0.5$ after ∼0.3 Gyr.

On another side, the bottom panel of Fig. 7, showing the mean line-of-sight velocity mapped within the inner 10 pc, evidences that the GC orbital evolution impinges a rotation along the 45 degree bisector of the x–y plane around the SMBH.

Such result is of particular interest in reference to the dynamics of stars around the SMBH hosted in the Andromeda galaxy nucleus, which has a mass of $M_{\rm SMBH} = (1.1–2.3) \times 10^8\,{\rm M}_\odot$ (Bender et al. 2005) and a lifetime $\gtrsim$100 Myr. Indeed, the Andomeda SMBH neighbourhood is characterized by the presence of a rotating, eccentric disc of stars (Lauer et al. 1993; Tremaine 1995), whose nature is still largely unclear. A better understanding of the origin of this discy structures may help in shedding light on the SMBH growth history and process (Hopkins & Quataert 2010a).

According to our present results, the infall of GCs seems to be inefficient in inducing the formation of such a configuration, at least when the central BH is very massive.

On the other hand, in our simulation all the GCs have initial distances to the galactic center larger than $\sim 10^2$ pc, and their disruption impinges only a mild rotation on the SMBH neighbourhood.

However, it is not clear whether a GC born close to the SMBH can give rise to a disc whose flatness survives for a time comparable to the estimated age (∼100 Myr) of the Andromeda nuclear stellar disc. In order to test such hypothesis, we made use of the data produced by Arca-Sedda et al. (2016).

In particular, one of their sets of simulations was characterized by a galaxy model (and central SMBH) equal to the one presented in this work, and a GC moving at an initial distance of 50 pc from the SMBH, i.e. smaller than those of the GCs in our numerical modelling, at varying GC initial eccentricity.

In the following, we refer to the simulation in which the GC moves on an orbit with $e_{\rm GC} \simeq 0.7$.

Using these data, we show in Fig. 8 the surface density map of the cluster after 100 Myr from the beginning of the simulation. It is quite evident the formation of a discy structure, with a projected radius extending up to ∼20 pc, slightly larger than M31 disc, which extends up to ∼8 pc. Moreover, the bright pixel evident at −20.5 pc is due to a bunch of bounded stars, debris of the GC core. The total mass of this structure is 400 $\,{\rm M}_\odot$, and has an extension of ∼0.02 pc.

This can be due to the GC model, which is based on a King density profile with $W_0 = 6$ and core radius $r_c = 0.24$ pc. A more concentrated system could preserve a rounder shape on a longer time-scale, due to the deeper potential well.

These results suggest that the origin of discy structures in the immediate surroundings of a SMBH can be ascribed to the disruption of a relatively young GC born deep into the galactic nucleus. It is worth noting that this scenario is complementary to another, suggested by some authors (Tremaine 1995; Hopkins & Quataert 2010b), according to which the disc forms from a rotating gas cloud that undergoes subsequent star formation episodes.

4.2 Tidal disruption events

During the life of a galaxy evolution, some stars can move sufficiently close to the SMBH to be completely disrupted. During these TDEs (Hills 1975), part of the gas coming from the shattered star feeds the SMBH and can give rise to a detectable burst of X-rays. Wang & Merritt (2004) investigated the secular role of stellar dynamics around SMBHs, showing that the typical TDE rate for a heavy galactic nucleus is limited to a few 10^{-4} yr^{-1} if the central SMBH exceeds $10^8\,{\rm M}_\odot$. In galaxies hosting SMBHs with masses 10^5–$10^7\,{\rm M}_\odot$, recently Stone, Küpper & Ostriker (2017) pointed out that in dense, pre-existing, NSCs TDE rates can be in the range 10^{-5}–10^{-3} yr^{-1}, in dependence on the NSC properties.

On the other hand, in galaxies characterized by a smooth, or cored, density profile hosting in their centre SMBH with mass above $10^8\,{\rm M}_\odot$ the TDE rate is generally limited in the range 10^{-6}–5×10^{-5} yr^{-1} (Stone & Metzger 2016). Note that our galaxy model represents this kind of galaxies, as its density inner slope is small, $\gamma = 0.1$.

In this section, we investigate whether the GC debris, which accumulates around the SMBH, can enhance the TDE rate in a galaxy characterized by a cored density profile.

A star with radius R_* and mass M_* orbiting an SMBH undergoes a TDE if it approaches the SMBH closer than the so-called Roche radius

$$r_{\rm R} = \eta R_* \left(\frac{M_{\rm SMBH}}{M_*}\right)^{1/3}, \tag{21}$$

with $\eta = 0.8$ (Merritt 2013). As said above, these TDEs are often followed by the emission of an X-ray flare with a time-scale of a few years. Nowadays, the detection of these strong signals represents a unique possibility to infer clues on the central SMBH mass and structure (Vinkó et al. 2015; Kochanek 2016; Metzger & Stone 2016; Yang et al. 2016).

In order to express the Roche radius in terms of the SMBH and stellar properties, we recall here that r_R is linked to the SMBH Schwarzschild's radius through the relation

$$\frac{r_{\rm R}}{r_{\rm S}} = 5.06 \left(\frac{M_*}{{\rm M}_\odot}\right)^{-1/3} \left(\frac{M_{\rm SMBH}}{10^7\,{\rm M}_\odot}\right)^{-2/3} \frac{R_*}{{\rm R}_\odot}. \tag{22}$$

Moreover, the mass and the radius of main-sequence stars are linked by a simple power law:

$$\frac{R_*}{{\rm R}_\odot} = \alpha \left(\frac{M_*}{{\rm M}_\odot}\right)^{\beta}, \tag{23}$$

with α and β depending on the stellar mass, as shown in Table 2

Table 2. Parameters linking stellar radii and masses.

	α	β
$M \leq 1.52\,M_\odot$	1.09	0.969
$M > 1.52\,M_\odot$	1.29	0.6035

(Demircan & Kahraman 1991; Gorda & Svechnikov 1998). Substituting into equation (22) we find:

$$\frac{r_R}{r_S} = 5.06 \left(\frac{M_{SMBH}}{10^7\,M_\odot}\right)^{-2/3} \alpha \left(\frac{M_*}{M_\odot}\right)^{-1/3+\beta}. \quad (24)$$

Assuming $M_{SMBH} = 10^8\,M_\odot$, equation (24) implies that stars with mass smaller than $0.88\,M_\odot$ undergo a direct plunge, and are wholly swallowed by the SMBH. This clearly poses a limit to the number and type of TDEs and subsequent X-ray bursts.

For instance, under the assumption that the galaxy nucleus can be described by an isothermal sphere, for an SMBH with mass $\sim 10^8\,M_\odot$ the expected rate of TDEs should be of the order of $10^{-4}\,M_\odot\ \mathrm{yr}^{-1}$ (Merritt 2013). Moreover, the TDE rate depends on the host galaxy density profile. Actually, while cored galaxies (inner slopes $\gamma < 0.5$) have TDE rates in the range $10^{-6} - 5 \times 10^{-5}\,M_\odot\ \mathrm{yr}^{-1}$, steeper power-law galaxies are characterized by larger TDE rates.

So, the condition for a given star to lead to a TDE is that $r_R/r_S \geq 1$ and the orbital pericentre, r_p, is $r_p \leq r_R$.

According to our model, the cumulative mass profile of the host galaxy is given by (Dehnen 1993)

$$M(r) = M_g \left(\frac{r}{r+r_g}\right)^{3-\gamma} \simeq M_g \left(\frac{r}{r_g}\right)^{3-\gamma}, \quad (25)$$

the latter relation being valid for $r \ll r_g$, i.e. in the vicinity of the SMBH influence radius. However, the GC infall changes the global density profile of the galaxy+GC system. As shown in Fig. 5, the density profile gets steeper towards the centre after $\gtrsim$200 Myr, with a slope determined by the GC orbital decay.

In particular, the density distribution at 220 Myr is sufficiently well fitted by a power law:

$$\rho(r) = \xi_0 r^{-\gamma_0}, \quad (26)$$

with $\gamma_0 = 0.62 \pm 0.06$ and $\xi_0 = 253 \pm 11\,M_\odot\ \mathrm{pc}^{-(3-\gamma_0)}$. Note that after the GC infall the value of γ has increased from 0.1 to 0.62, a value that places our model slightly above that of the group of 'intermediate cusp' galaxy (with $0.3 < \gamma < 0.5$; Stone & Metzger 2016).

Integration gives the cumulative, inner, mass distribution

$$M_f(r) = 4\pi \int_0^r r^2 \rho(r) \mathrm{d}r = \frac{4\pi\xi_0}{3-\gamma_0} r^{3-\gamma_0}. \quad (27)$$

leading to a ratio between the final and initial mass radial profiles which is

$$\frac{M_f(r)}{M(r)} = \frac{4\pi\xi_0}{(3-\gamma_0)M_g} \frac{r^{\gamma-\gamma_0}}{r_g^{\gamma-3}}. \quad (28)$$

Substituting in equation (28), the relevant quantities discussed above we find that the above mass ratio attains a value of $\sim 2 \times 10^3$ at $r = 10^{-3}$ pc. Due to that the TDE rate is proportional to the galaxy density (Wang & Merritt 2004), we expect that $\dot{N}_{TDE}$ after the GC infall would thus increase by a factor of $\sim 10^3$. As said above, a correct analysis of possible TDEs must account only for stars moving on orbits whose pericentres fall below r_R and mass greater than $0.88\,M_\odot$.

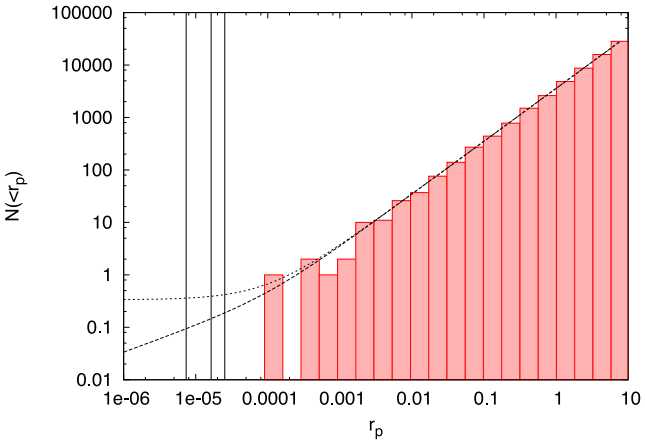

Figure 9. Cumulative distribution of the stars pericentre. From left to right, the black vertical lines represent the Roche radius for a 0.5, 2 and $10\,M_\odot$ star. The two black curves represent the fitting functions described in equations (33) and (34).

As discussed in Section 3.1, in our model the SMBH influence radius is $\gtrsim$10 pc, significantly larger than r_R.

We consider stars formerly belonging to GCs and which are now buzzing around the SMBH, we can evaluate their orbital pericentres, r_p, in the two-body approximation:

$$r_p = (1-e_*)\frac{1}{2/r - v_*^2/(GM_{SMBH})}; \quad (29)$$

This approximation is valid because these stars are confined in the SMBH influence sphere whose radius is $\sim$13. For this reason, we can substitute $v_*^2/(GM_{SMBH})$ with r_{inf} in the equation above to obtain

$$r_p = \frac{1-e_*}{2-r/r_{inf}} r. \quad (30)$$

all the stars that will likely undergo a TDE are those moving in the inner region around the SMBH, at distances below 10^{-3} pc. These stars are debris of the dissolved population of GCs, and their orbital apocentre hardly can exceed the SMBH influence radius, which is $\sim$13 pc by the end of our simulation. Hence, we can substitute $\sigma_g^2/(GM_{SMBH}$ with r_{inf} in the equation above to obtain

$$r_p = \frac{1-e_*}{2-r/r_{inf}} r. \quad (31)$$

To have a TDE, the condition $r_p \leq r_R$ leads to

$$r_p \leq \frac{2r_R}{1-e_*+r_R/r_{inf}} \simeq \frac{r_R}{1-e_*}. \quad (32)$$

Hence, even for very eccentric orbit, the star distance to the SMBH must be small (less than $10r_R$ for $e_* = 0.9$), too small to be resolved with our simulation, despite its high level of detail.

For a Sun-like star, the pericentre threshold to have a TDE corresponds, roughly, to 10^{-5} pc, increasing up to a few 10^{-4} in the case of a $100\,M_\odot$ star, at least one order of magnitude smaller than our simulation resolution. Nevertheless, we can use our results to extrapolate the number of stars expected to undergo a TDE in a real galaxy.

In Fig. 9, the cumulative distribution $N(< r_p)$ of the stars pericentre is shown. In order to give an estimate of the total number of stars that can be disrupted by the SMBH tidal force, we should extrapolate this distribution towards small values of r_p.

Table 3. Parameters of the N_{r_p} fitting functions.

	a	b	c
$f_1(r_p)$	10^4	0.507 ± 0.003	34 ± 1
$f_2(r_p)$	10^4	1.007 ± 0.003	0.33 ± 0.01

Due to the limited resolution of our N-body simulation, below 10^{-3} pc, we cannot state clearly whether the low-end tail of N_{r_p} tends to a constant value or rapidly drops to zero, giving a huge uncertainty in the extrapolation procedure. Due to this, we decided to search for two different fitting functions, able to reproduce the two extreme cases of (1) an N_{r_p} that drops rapidly to 0 at decreasing pericentre, on one side, and that of (2) an N_{r_p} that tends to a constant at small values of r_p.

The rapidly decreasing function (1), named f_1, is defined as

$$f_1(r_p) = kc(ar_p + 1)^b \sqrt{r_p}, \tag{33}$$

while the other function, f_2, is given by

$$f_2(r_p) = kc(ar_p + 1)^b, \tag{34}$$

In both equations, shown in Fig. 4, $k = 1/N_{\rm GCS}$ represents the inverse of the number of particles used to represent all the GCs. Moreover, we set $1/a = 10^{-4}$ pc, which is the length-scale below which our resolution in N_{r_p} loses quality.

Once the two functions have been selected, we used the non-linear least-squares (NLLS) Marquardt–Levenberg algorithm implemented in the analysis tool GNUPLOT, to provide the set of parameters that describe at best the N_{r_p}.

The value of the fitting parameters are resumed in Table 3.

Among all the stars, those having an angular momentum smaller than a limiting value, called loss-cone angular momentum $L_{\rm LC} = \sqrt{GM_{\rm SMBH} r_R}$, will undergo a TDE over a relaxation time (Rees 1988; Merritt 2013). Following Wang & Merritt (2004), only stars having pericentres smaller than a critical radius, $r_{\rm crit}$, have orbital properties that can cause the deflection of stars into the loss-cone regime. According to their definition, the TDE rate is given by the ratio between the number of stars having a pericentre smaller than $r_{\rm crit}$ and the local relaxation time calculated at this radius

$$\dot{N}_{\rm TDE}(<r_{\rm crit}) = \frac{N_{\rm TDE}(<r_{\rm crit})}{T_r(r < r_{\rm crit})}, \tag{35}$$

where $N_{\rm TDE}(<r_{\rm crit})$ represent the number of stars having pericentre smaller than $r_{\rm crit}$, and where we used the two-body relaxation time-scale as defined by Spitzer & Harm (1958)

$$T_r(r) = \frac{\sqrt{2}\sigma_g(r)^3}{\pi G^2 m_* \rho(r) \ln \Lambda}. \tag{36}$$

In order to calculate $r_{\rm crit}$, we must set the so-called *loss-cone angle*, $\theta_{\rm LC}$

$$\theta^2_{\rm LC} = r_R / r_{\rm crit}, \tag{37}$$

to be equal to the angle, θ_d, by which a star orbit is deflected into the loss-cone, which is the ratio between the star orbital period and the local relaxation time-scale

$$\theta^2_d = \frac{\sqrt{r^3_{\rm crit}/GM_{\rm SMBH}}}{T_r(r_{\rm crit})}. \tag{38}$$

The condition $\theta_d = \theta_{\rm LC}$ implies

$$r^{5/2-\gamma_0}_{\rm crit} = \frac{\sqrt{2}\eta\alpha M^{5/6}_{\rm SMBH} m_*^{-4/3+\beta}\sigma_g^3}{\pi \ln \Lambda \xi_0}. \tag{39}$$

Table 4. Fraction of heavy stars at different times.

T Gyr	$m_e(Z_\odot = 0.02)$ $M_\odot$	$m_e(Z_\odot = 0.0004)$ $M_\odot$	$n(m > 1\,M_\odot)$ (per cent)
0	100	100	4.5
0.01	17	19	4.4
0.03	9.2	9.3	4.3
0.3	4	4.5	3.8
1	2.5	2.0	3.2

Col. 1: time. Col. 2: minimum unevolved mass at solar metallicity. Col. 3: minimum unevolved mass at metallicity $Z = 0.0004$. Col. 4: fraction of stars with mass larger than $1\,M_\odot$.

Given the dependence of the Roche radius on the star mass (see equation 22), to get the fraction of stars that likely to undergo TDE we need to know the GC mass function.

Assuming a Salpeter initial mass function (Salpeter 1955), the fraction of stars having a mass greater than the limiting value above which the pericentre distance to the SMBH is smaller than its Roche radius is given by

$$\nu(r_p < r_R, \tau = 0) = \frac{m_M^{1-s} - m_p^{1-s}}{m_M^{1-s} - m_m^{1-s}}, \tag{40}$$

where m_p is the star mass that gives $r_R = r_p$, $s = 2.35$ and $m_m = 0.1\,M_\odot$ is the minimum mass and $m_M = 100\,M_\odot$ the maximum mass in the IMF (age zero, i.e. $\tau = 0$).

To account for the time evolution of the MF due to star mass-loss, to evaluate the proper value of ν, we followed the procedure described in Arca-Sedda (2016), which makes use of the stellar evolution code SSE (Hurley, Pols & Tout 2000). Following the time evolution of the population of stars with masses in the range $m_m - m_M$ up to 1 Gyr, we found that the evolved MF shows at any time a steep decline at masses above m_e defined as the mass of stars ending their H burning phase at that time (it represents the minimum mass of unevolved stars at a given age).

We report in Table 4 some values of m_e at different times, highlighting the fraction of stars heavier than $1\,M_\odot$. We gave estimate assuming for the GCs either a solar metallicity, $Z_\odot = 0.02$, or a low value, $Z_\odot = 0.0004$, typical of old GCs in the MW.

Note that in the range of ages of Table 4, m_e is such to give a Roche radius greater than the SMBH r_S.

Finally, in our simulation, the fraction of stars which may give origin to TDEs is given by

$$f_{\rm TDE}(<r_p) = f_i(r_p)\nu(r_R > r_p, \tau), \tag{41}$$

where f_i, $i = 1, 2$ are the functions in equations (33) and (34). The choice $f_1(r_R)$ minimizes the fraction of TDEs, while $f_2(r_R)$ maximizes it. In Fig. 10, we show how $f_{\rm TDE}$ varies as a function of the pericentre distance to the galactic centre assuming different values of the GC age.

Therefore, the TDE rate can be evaluated substituting $r_{\rm crit}$ in equation (35) and using equation (41):

$$\dot{N}_{\rm TDE}(<r_{\rm crit}) = \frac{f_{\rm TDE}(<r_{\rm crit})N_*}{T_r(r_{\rm crit})}. \tag{42}$$

In our calculations, we considered a total number of stars $N_* \simeq 2 \times 10^{11}$, a velocity dispersion $\sigma_g(r) \sim 100\,{\rm km\,s^{-1}}$, as evaluated in our simulation at distances below 1 pc from the SMBH, and a density at $r \sim 10^{-5}$ pc given by $\rho(r) \simeq 3 \times 10^5\,M_\odot\,{\rm pc^{-3}}$, as evaluated by equation (26). Note that $r_p > 10^{-5}$ pc is the minimum distance above which pericentre of the stars is larger than the SMBH

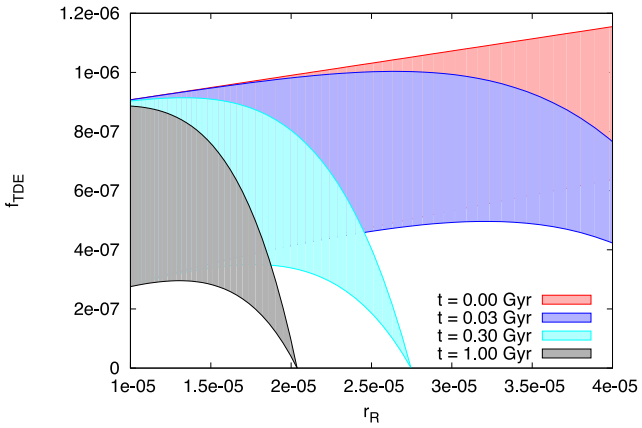

Figure 10. Total fraction of stars with Roche radius larger than their pericentre, $r_p < r_R$. The lower limit of the shaded region is obtained assuming in our calculation $f_1(r_p)$, while the upper limit is obtained assuming $f_2(r_p)$.

Schwarzschild radius, thus representing the spatial region where the probability to have a TDE is maximized.

By substituting the relevant quantities, we found a TDE rate $\dot{N}_{\rm TDE} = 1.9 \times 10^{-4}$ yr^{-1}. We note here that galaxies with γ in the range 0.3–0.8 and SMBHs with masses $\sim 10^8$ M$_\odot$ are characterized by a TDE rate $\simeq$(1.9–4.5) $\times$ 10^{-5} yr^{-1} (cfr. table 1 in Stone & Metzger (2016)), which is an order of magnitude lower than what we found in our simulations, which is characterized by $\gamma \sim 0.6$. Additionally, it seems that the mass accumulated around the SMBHs in form of stellar debris can actually determine an enhancement in the TDE rate. Anyway, the above result depends of various assumptions, as discussed in the following subsection. This is particularly interesting in the context of the recent discovery of a large TDE rate in the E+A galaxy NGC3156. E+A galaxies are elliptical galaxies that underwent a starburst formation episode 0.1–1 Gyr ago and are often populated by a population of young massive clusters (Yang et al. 2004). NGC3156 is characterized by an SMBH significantly lighter than that of our model, with a mass 0.9–2.7 $\times$ 10^6 M$_\odot$ (Stone & van Velzen 2016). Assuming that the TDE rate is linked to the SMBH mass through a power law (Stone & Metzger 2016), we can rescale our results to the SMBH mass of NGC3516 getting a TDE rate $\dot{N}_{\rm TDE} = (0.6-1.1) \times 10^{-3}$ yr^{-1}, compatible with the observed estimated value, thus suggesting that the infall and merger of a population of young star clusters can significantly enhance the TDE rate.

Caveats of the TDE calculation

The results obtained for TDE rates depend strongly on the galaxy model and the GC masses and orbital properties. In our calculations, the main parameters that affect the TDE rate are (i) the GC position and orbital velocity distributions and (ii) the GC mass function and total number.

Regarding the first point, we assumed that the GC and host galaxy distributions does not differ significantly. Such simple assumption allows us to explain several properties of galactic centres, for instance the masses and sizes of NCs (Antonini 2013; Arca-Sedda & Capuzzo-Dolcetta 2014b; Gnedin et al. 2014), the γ-ray flux observed in the Milky Way central regions (Brandt & Kocsis 2015) and the presence of an old population of red giant stars in the Milky Way NC (Minniti et al. 2016). A GC density profiles steeper than the galaxy would lead to too large NCs, due to the high efficiency of df in the galaxy centre vicinity, while shallower density profiles would lead to too small NCs, as in this case most of the GCs can be disrupted by the galactic tidal forces.

Regarding the second point, the total mass in massive ($M > 10^5$ M$_\odot$) star clusters in a heavy galaxy is roughly 0.1–1 per cent of the galaxy mass (Harris 2010). Assuming that GC masses range in between (0.3 and 2) $\times$ 10^6 M$_\odot$ and that they are distributed according to the background galaxy distribution, we expect, for a 10^{11} M$_\odot$ galaxy, between 8 and 80 GCs within 100 pc from the SMBH. Therefore, it seems that $\gtrsim$40 GCs is a reasonable choice, given our current knowledge of galaxy formation and evolution. Our choice of the GC minimum and maximum mass allowed is dictated by the computational need of having a sufficient number of particles to represent the smallest clusters. However, such choice is well supported by previous theoretical works that tackled similar problems (see for instance Antonini 2013, Arca-Sedda & Capuzzo-Dolcetta 2014b and Gnedin et al. 2014). Moreover, our simulation shows that only 16 GCs, out of the 42, reach the inner 10 pc (see Fig. 3) and undergo a strong encounter with the SMBH. The remaining clusters are subjected to the strong action of the galactic tidal field, and never approach close to the galactic centre, thus they do not contribute to the density enhancement that leads to the increase in the TDE rate.

5 CONCLUSIONS

In this paper, we modelled the evolution of 42 GCs moving in the nucleus of a massive galaxy hosting a 10^8 M$_\odot$ SMBH at its centre. This was done self-consistently, by mean of a numerical representation at an unprecedented level of detail in this framework. The simulation outcomes show that tidal torques due to the combined effect of the background galaxy and SMBH shape the properties of the SMBH surroundings, eroding the infalling GCs and quenching the formation of a dense nucleus.

Indeed, although the GC orbital decay leads to an increase in the galactic spatial density, it is not sufficiently efficient to produce a clear enhancement of the central surface density profile, which is widely used to infer the presence of an NSC.

Using the output of our simulations, we also investigated the role of SMBH–GC interactions in determining stellar TDE rates.

The main outcomes of this paper can be summarized as follows:

(i) we found that tidal forces and dynamical friction acts rapidly in determining the GC evolution, suggesting that GC–SMBH interactions can shape a galactic nucleus on time-scales smaller than 1 Gyr;

(ii) the tidal torques induced by the central SMBH on its surroundings are such to shatter most of the GCs that approach the galactic central region, causing an inefficient deposit of mass, in the form of GC debris, around the SMBH. This provide a reliable explanation for the absence of NSC in galaxies hosting SMBHs heavier than 10^8 M$_\odot$, as outlined in other recent papers (Antonini 2013; Arca-Sedda & Capuzzo-Dolcetta 2014b; Arca-Sedda et al. 2016);

(iii) the GC debris accumulated around the SMBH impinge a clear kinematic fingerprint on the galactic nucleus. In particular, our results show that the innermost region around the SMBH is characterized by a flattened configuration, strongly triaxial and weakly rotating;

(iv) the interaction among the SMBH, the stellar field and the infalling 42 GCs significantly shapes the GC mass distribution. In particular, GC mass-loss induced by tidal forces leads to a subpopulation of GCs with masses below 3×10^4 M$_\odot$, moving at $\sim$50–100 pc from the galactic centre. Above such limiting value, their

mass distribution is well described by a power law, characterized by a slope $\simeq -0.8$;

(v) comparing our results with Arca-Sedda et al. (2016), we note here that if a massive cluster forms in the SMBH vicinity, its disruption can lead to the formation of a discy structure with a lifetime $\simeq$100 Myr. This provide a further explanation for the origin of dense stellar discs around SMBHs with masses around $10^8\,M_\odot$, as observed, for instance, in the M31 galaxy (Lauer et al. 1993; Tremaine 1995);

(vi) using the huge amount of data produced by our simulation, we investigated whether GCs–SMBH interactions can enhance the probability of flares from tidally destroyed stars belonging to GCs passing by the SMBH. We found a TDE rate of $\sim 1.9 \times 10^{-4}$ yr^{-1}, a value significantly larger than what expected for galaxies characterized by a similarly steep density profile (Stone & Metzger 2016), which finds an interesting agreement in recent observations of several E+A galaxies (Stone & van Velzen 2016).

ACKNOWLEDGEMENTS

The authors acknowledge the referee, whose helpful comments and suggestions allowed to improve an earlier version of the manuscript. MAS acknowledges Sapienza, University of Rome, which funded the research programme 'MEGaN: modelling the evolution of galactic nuclei' via the grant 52/2015, and the Sonderforschungsbereich SFB 881 'The Milky Way System' of the German Research Foundation (DFG) for the financial support provided. MAS also thanks the Zentrum fur Astronomie – Astronomisches Rechen-Institut of Heidelberg for the hospitality during the development of part of this research.

REFERENCES

Aharon D., Perets H. B., 2015, ApJ, 799, 185
Antonini F., 2013, ApJ, 763, 62
Antonini F., Merritt D., 2012, ApJ, 745, 83
Antonini F., Capuzzo-Dolcetta R., Mastrobuono-Battisti A., Merritt D., 2012, ApJ, 750, 111
Antonini F., Barausse E., Silk J., 2015, ApJ, 812, 72
Arca-Sedda M., 2016, MNRAS, 455, 35
Arca-Sedda M., Capuzzo-Dolcetta R., 2014a, ApJ, 785, 51
Arca-Sedda M., Capuzzo-Dolcetta R., 2014b, MNRAS, 444, 3738
Arca-Sedda M., Capuzzo-Dolcetta R., 2016, MNRAS, 461, 4335
Arca-Sedda M., Capuzzo-Dolcetta R., 2017, MNRAS, 464, 3060
Arca-Sedda M., Capuzzo-Dolcetta R., Antonini F., Seth A., 2015, ApJ, 806, 220
Arca-Sedda M., Capuzzo-Dolcetta R., Spera M., 2016, MNRAS, 456, 2457
Bekki K., 2007, PASA, 24, 77
Bekki K., Graham A. W., 2010, ApJ, 714, L313
Bender R. et al., 2005, ApJ, 631, 280
Böker T., Laine S., van der Marel R. P., Sarzi M., Rix H.-W., Ho L. C., Shields J. C., 2002, AJ, 123, 1389
Böker T., Sarzi M., McLaughlin D. E., van der Marel R. P., Rix H.-W., Ho L. C., Shields J. C., 2004, AJ, 127, 105
Bonfini P., Graham A. W., 2016, ApJ, 829, 81
Brandt T. D., Kocsis B., 2015, ApJ, 812, 15
Capuzzo-Dolcetta R., 1993, ApJ, 415, 616
Capuzzo-Dolcetta R., Fragione G., 2015, MNRAS, 454, 2677
Capuzzo-Dolcetta R., Miocchi P., 2008, MNRAS, 388, L69
Capuzzo-Dolcetta R., Spera M., Punzo D., 2013, J. Comput. Phys., 236, 580
Chandar R., Leitherer C., Tremonti C., Calzetti D., 2003, ApJ, 586, 939
Chandrasekhar S., 1943, ApJ, 97, 255
Côté P. et al., 2006, ApJS, 165, 57
Davies M. B., Miller M. C., Bellovary J. M., 2011, ApJ, 740, L42
Dehnen W., 1993, MNRAS, 265, 250
Demircan O., Kahraman G., 1991, Ap&SS, 181, 313
den Brok M. et al., 2014, MNRAS, 445, 2385
Dosopoulou F., Antonini F., 2017, ApJ, 840, 31
Dressler A., Gunn J. E., 1983, ApJ, 270, 7
Emsellem E., 2013, MNRAS, 433, 1862
Erwin P., Gadotti D. A., 2012, Adv. Astron., 2012, 946368
Ferrarese L. et al., 2006, ApJ, 644, L21
Fragione G., Capuzzo-Dolcetta R., Kroupa P., 2017, MNRAS, 467, 451
Franx M., Illingworth G., Heckman T., 1989, AJ, 98, 538
Georgiev I. Y., Böker T., 2014, MNRAS, 441, 3570
Georgiev I. Y., Böker T., Leigh N., Lützgendorf N., Neumayer N., 2016, MNRAS, 457, 2122
Gnedin O. Y., Ostriker J. P., Tremaine S., 2014, ApJ, 785, 71
Gorda S. Y., Svechnikov M. A., 1998, Astron. Rep., 42, 793
Graham A. W., 2012, MNRAS, 422, 1586
Graham A. W., Spitler L. R., 2009, MNRAS, 397, 2148
Graham A. W., Onken C. A., Athanassoula E., Combes F., 2011, MNRAS, 412, 2211
Harris W. E., 2010, Phil. Trans. R. Soc. A, 368, 889
Hills J. G., 1975, Nature, 254, 295
Hopkins P. F., Quataert E., 2010a, MNRAS, 405, L41
Hopkins P. F., Quataert E., 2010b, MNRAS, 407, 1529
Hurley J. R., Pols O. R., Tout C. A., 2000, MNRAS, 315, 543
King I., 1962, AJ, 67, 471
King I. R., 1966, AJ, 71, 64
King A., 2003, ApJ, 596, L27
King A., 2005, ApJ, 635, L121
Kochanek C. S., 2016, MNRAS, 461, 371
Kormendy J., Ho L. C., 2013, ARA& A, 51, 511
Lauer T. R. et al., 1993, AJ, 106, 1436
Leigh N., Böker T., Knigge C., 2012, MNRAS, 424, 2130
McLaughlin D. E., King A. R., Nayakshin S., 2006, ApJ, 650, L37
Mastrobuono-Battisti A., Perets H. B., Loeb A., 2014, ApJ, 796, 40
Melo I. T. e., Capuzzo-Dolcetta R., 2016, J. Phys. Conf. Ser., 689, 012008
Merritt D., 2006, ApJ, 648, 976
Merritt D., 2013, Dynamics and Evolution of Galactic Nuclei. Princeton Univ. Press, Princeton, NJ
Metzger B. D., Stone N. C., 2016, MNRAS, 461, 948
Milosavljević M., 2004, ApJ, 605, L13
Minniti D., Contreras Ramos R., Zoccali M., Rejkuba M., Gonzalez O. A., Valenti E., Gran F., 2016, ApJ, 830, L14
Nayakshin S., Wilkinson M. I., King A., 2009, MNRAS, 398, L54
Neumayer N., Walcher C. J., 2012, Adv. Astron., 2012
Nguyen D. D., Seth A. C., Reines A. E., den Brok M., Sand D., McLeod B., 2014, ApJ, 794, 34
Perets H. B., Mastrobuono-Battisti A., 2014, ApJ, 784, L44
Petts J. A., Read J. I., Gualandris A., 2016, MNRAS, 463, 858
Quintero A. D. et al., 2004, ApJ, 602, 190
Rees M. J., 1988, Nature, 333, 523
Reines A. E., Deller A. T., 2012, ApJ, 750, L24
Rossa J., van der Marel R. P., Böker T., Gerssen J., Ho L. C., Rix H.-W., Shields J. C., Walcher C.-J., 2006, AJ, 132, 1074
Salpeter E. E., 1955, ApJ, 121, 161
Scott N., Graham A. W., 2013, ApJ, 763, 76
Seth A., Agüeros M., Lee D., Basu-Zych A., 2008, ApJ, 678, 116
Shankar F., Weinberg D. H., Miralda-Escudé J., 2009, ApJ, 690, 20
Spitzer L., Jr, Harm R., 1958, ApJ, 127, 544
Stone N. C., Metzger B. D., 2016, MNRAS, 455, 859
Stone N. C., van Velzen S., 2016, ApJ, 825, L14
Stone N. C., Küpper A. H. W., Ostriker J. P., 2017, MNRAS, 467, 4180
Tremaine S. D., 1976, ApJ, 203, 345
Tremaine S., 1995, AJ, 110, 628
Turner M. L., Côté P., Ferrarese L., Jordán A., Blakeslee J. P., Mei S., Peng E. W., West M. J., 2012, ApJS, 203, 5

Urry C. M., Padovani P., 1995, PASP, 107, 803
van den Bosch R. C. E., Gebhardt K., Gültekin K., van de Ven G., van der Wel A., Walsh J. L., 2012, Nature, 491, 729
Vinkó J. et al., 2015, ApJ, 798, 12
Walcher C. J., Böker T., Charlot S., Ho L. C., Rix H.-W., Rossa J., Shields J. C., van der Marel R. P., 2006, ApJ, 649, 692
Wang J., Merritt D., 2004, ApJ, 600, 149
Yang Y., Zabludoff A. I., Zaritsky D., Lauer T. R., Mihos J. C., 2004, ApJ, 607, 258
Yang J., Paragi Z., van der Horst A. J., Gurvits L. I., Campbell R. M., Giannios D., An T., Komossa S., 2016, MNRAS, 462, L66
Zabludoff A. I., Zaritsky D., Lin H., Tucker D., Hashimoto Y., Shectman S. A., Oemler A., Kirshner R. P., 1996, ApJ, 466, 104

SUPPORTING INFORMATION

Supplementary data are available at *MNRAS* online.

video_MEGAN_P1.mp4

Please note: Oxford University Press is not responsible for the content or functionality of any supporting materials supplied by the authors. Any queries (other than missing material) should be directed to the corresponding author for the article.

This paper has been typeset from a TEX/LATEX file prepared by the author.